

Atomistic Studies of Nanosized Copper Structures

Atomistic Studies of Nanosized Copper Structures

Dan Johansson



LUND
UNIVERSITY

DOCTORIAL DISSERTATION

by due permission of the Faculty of Engineering, Lund University, Sweden
to be defended at lecture hall M:E, M-building, LTH, Ole Römers väg 1,
221 00, Lund
on October 21st 2016 at 10:15 a.m.

Faculty opponent

Dr. Vitaly Kuzkin

Deputy Head of Department of Theoretical and Applied Mechanics, Peter the
Great St.Petersburg Polytechnic University, St. Petersburg, Russia.

| | | |
|--|-------------------------|---|
| Organization Division of Mechanics Lund University P.O. Box 118 SE-221 00 Lund Sweden | | Document name DOCTORIAL DISSERTATION |
| | | Date of issue October 21 st 2016 |
| Author(s) Dan Johansson | | Supervisors Professor Solveig Melin Associate professor Per Hansson |
| Title Atomistic Studies of Nanosized Copper Structures | | |
| Abstract <p>In contrast to macrosized structures, for nanosized structures the fraction of surface atoms is not negligible. Furthermore, as the size decreases the idea that matter are homogeneous and continuous breaks down and cannot be applied. These facts lead to that the material properties on the nanoscale deviate from the material properties on the macroscale.</p> <p>The modern information society arose from, and demands, devices that supply fast and easy accessible ways of communication, e.g. computers, cell phones, satellites, etc. Such devices are often made out of thousands of micro- and nanosized electrical components. To produce micro- and nanosized components, sophisticated measuring tools and manufacturing robots with nanoprecision are needed. Thus, the modern society depends on devices that consist of structures that have properties that are determined on the nanoscale.</p> <p>Due to its low resistivity and ability to handle high currents, copper is an element of large interest in the nanoelectro-mechanical industry. The research work presented in this dissertation aims to increase the understanding in nanosized copper structures and to investigate how well continuum theory applies in the vicinity of nanosized crack shaped voids. To achieve this, nanosized copper structures have been simulated with molecular dynamics.</p> <p>Part I of this thesis gives a short introduction of the topic followed by problem formulations, a brief introduction to molecular dynamics and a short summary of the results and conclusions. In Part II, the five papers that constitute the bulk of this thesis are appended.</p> | | |
| Keywords molecular dynamics, copper, void, stress, strain, silicon, shear anisotropy | | |
| Classification system and/or index terms (if any) | | |
| Supplementary bibliographical information | | Language English |
| ISSN and key title | | ISBN 978-91-7623-956-8 (print) 978-91-7623-957-5 (pdf) |
| Recipient's notes | Number of pages 116 | Price |
| | Security classification | |

I, the undersigned, being the copyright owner of the abstract of the above-mentioned dissertation, hereby grant to all reference sources the permission to publish and disseminate the abstract of the above-mentioned dissertation.

Signature *Dan Johansson*

Date 2016-9-14

Atomistic Studies of Nanosized Copper Structures

Dan Johansson



LUND
UNIVERSITY

Copyright © Dan Johansson and Division of Mechanics

Division of Mechanics, Department of Mechanical Engineering,
Faculty of Engineering, Lund University

ISBN: 978-91-7623-956-8 (print)

ISBN: 978-91-7623-957-5 (pdf)

Printed in Sweden by Media-Tryck, Lund University
Lund 2016



To Alice

Acknowledgements

The work presented in this doctoral thesis has been carried out at the Division of Mechanics, Lund University and was funded by the Swedish Research Council. Working as a PhD student has been a great learning experience since it has offered both personal development and the opportunity to enhance my analytical skills. As a PhD student, the workload has sometimes been very high and stressful. Even so, my time as a PhD student has given me a lot of fun and sometimes weird memories that I will keep laughing at and enjoy until the day my heart stops beating.

I would like to thank my two supervisors professor Solveig Melin and associate professor Per Hansson for their benevolence, encouragement, and guidance in my work. I would also like to thank the department's administrative manager and IT-manager Rosé-Marie Hermansson and Johan Persson, respectively, associate professor Aylin Ahadi and associate professor Kristina Nilsson in general and professor Srinivasan Iyengar and associate professor Per Lidström especially for always taking the time in their busy schedules to try to answer my questions.

Finally I would like to thank my family for their support. Especially my fiancée Frida for her unconditional love and ability to always stay warm, caring, and cheerful.

Lund, August 2016

Dan Johansson

Abstract

In contrast to macrosized structures, for nanosized structures the fraction of surface atoms is not negligible. Furthermore, as the size decreases the idea that matter are homogeneous and continuous breaks down and cannot be applied. These facts lead to that the material properties on the nanoscale deviate from the material properties on the macroscale.

The modern information society arose from, and demands, devices that supply fast and easy accessible ways of communication, e.g. computers, cell phones, satellites, etc. Such devices are often made out of thousands of micro- and nanosized electrical components. To produce micro- and nanosized components, sophisticated measuring tools and manufacturing robots with nanoprecision are needed. Thus, the modern society depends on devices that consist of structures that have properties that are determined on the nanoscale.

Due to its low resistivity and ability to handle high currents, copper is an element of large interest in the nanoelectro-mechanical industry. The research work presented in this dissertation aims to increase the understanding in nanosized copper structures and to investigate how well continuum theory applies in the vicinity of nanosized crack shaped voids. To achieve this, nanosized copper structures have been simulated with molecular dynamics.

Part I of this thesis gives a short introduction of the topic followed by problem formulations, a brief introduction to molecular dynamics and a short summary of the results and conclusions. In Part II, the five papers that constitute the bulk of this thesis are appended.

Sammanfattning

Till skillnad från makrokomponenter så är andelen ytatomer inte negligerbar i nanokomponenter. Därtill, när en komponents storlek minskar ner på nanonivå fallerar idén om att materialet är homogent och kontinuerligt. Allt detta resulterar i att egenskaperna som ett material har på nanonivå skiljer sig från de egenskaper som materialet har på makronivå.

Det moderna informationssamhället som vi lever i uppstod som en följd av tillgängligheten av apparater såsom datorer, mobiltelefoner, satelliter etc. som möjliggör och tillgodoser snabb och lättillgänglig kommunikation. Dessa apparater består ofta av tusentals mikro- och nanoelektroniska komponenter. För att tillverka mikroelektriska och nanoelektriska kretsar krävs avancerad mätutrustning och tillverkningsrobotar med nanoprecision. Således är det moderna samhället beroende av apparater som har egenskaper som bestäms på nanonivå.

På grund av sin låga resistivitet och förmåga att leda starka strömmar är grundämnet koppar ett högtintressant material för den elektromekaniska nanoindustrin. Forskningsarbetet som presenteras i den här doktorsavhandlingen har som mål att öka förståelsen för kopparkomponenter på nanonivå samt undersöka hur pass väl brottmekanik och finita element metoden, som båda förutsätter ett kontinuum, kan beskriva spänningarna och töjningarna, eller snarare atomförflyttningarna, i närheten av nanosprickor. För att åstadkomma detta har nanokomponenter av koppar simulerats med hjälp av molekylodynamik.

Del I i den här avhandlingen inleds med en kort introduktion till ämnet och därefter följer problemformuleringarna, en kort introduktion till molekylodynamik, en kort sammanfattning av forskningsresultaten samt slutsatser. I Del II är de fem artiklarna som utgör huvuddelen av den här avhandlingen bifogade.

List of papers

The bulk of the thesis is based on the five papers listed below. In each and every paper, the author *Dan Johansson* has written the text and carried out all programming, the computer simulations, the post-processing of the out-put data, and analyzed the results. In Paper I, II, and III, and to some extent also Paper IV, the author's supervisors played an important role in planning the research, giving important inputs and proofreading. Considering Paper V, all planning etc. has been carried out by the author and the supervisors have contributed in discussion and proofreading.

- I **Stress analysis around a through crack shaped void in a single crystal copper strip coated on an infinitely stiff material using molecular dynamics.**
Dan Johansson, Per Hansson, and Solveig Melin
Engineering Fracture Mechanics, vol. 116, pp. 58-68, 2014
- II **Stress analysis of highly constrained copper strips with through crack shaped voids using molecular dynamics.**
Dan Johansson, Per Hansson, and Solveig Melin
Key Engineering Materials, vol. 592-593, pp. 43-46, 2013
- III **Stress and displacement configurations in the vicinity of a void in a nanometer copper strip.**
Dan Johansson, Per Hansson, and Solveig Melin
Engineering Fracture Mechanics, vol. 152, pp. 139-146, 2016
- IV **Lattice optimization of Si-Cu interfaces on atomic scale.**
Dan Johansson, Per Hansson, and Solveig Melin
Submitted to Computational Material Science
- V **Shear anisotropy in Si-Cu interfaces on the atomic scale.**
Dan Johansson and Per Hansson
Submitted to Computational Material Science

Contents

| | |
|--|-----------|
| <i>Acknowledgements</i> | ix |
| <i>Abstract</i> | xi |
| <i>Sammanfattning</i> | xiii |
| <i>List of papers</i> | xv |
| I COMPREHENSIVE SUMMARY | 1 |
| 1 Introduction | 3 |
| 1.1 Background | 4 |
| 2 Objectives | 7 |
| 3 Atomic simulations | 9 |
| 3.1 Governing equations | 10 |
| 3.2 Potentials | 11 |
| 3.2.1 The Lennard-Jones potential | 12 |
| 3.2.2 The Modified embedded atom method | 12 |
| 3.3 Periodic boundary conditions | 13 |
| 4 Problem formulations | 15 |
| 4.1 Lattice structure and anisotropy in copper and silicon | 15 |
| 4.2 The flawed copper strip | 17 |
| 4.3 The copper coated silicon film | 19 |
| 5 Results | 21 |
| 5.1 Main results in Papers I, II, and III | 21 |
| 5.2 Main results in Papers IV and V | 25 |
| 6 Conclusions | 31 |
| References | 33 |
| II APPENDED PAPERS | 41 |
| Paper I | 43 |
| Paper II | 57 |

| | |
|------------------|-----------|
| Paper III | 63 |
| Paper IV | 73 |
| Paper V | 87 |

Part I

**COMPREHENSIVE
SUMMARY**

Chapter 1

Introduction

Since the dawn of mankind the knowledge in material science in terms of material properties and how to produce it (initially where to find it) has been fundamental to the development of civilization. Anthropologists have defined four historical epochs by the materials that were commonly used among the civilizations during those eras, e.g. the Stone, Copper, Bronze, and Iron ages. Different culture groups' progressions towards more sophisticated materials have correlated with their societies different levels of innovation and the local availability of materials. The more advanced materials a society could produce, the higher standard of living got its citizens^{1,2}.

In our everyday life we encounter appliances that are made of a wide range of different engineering materials such as metals, plastics and ceramics. Some of these appliances are large, e.g. the engine block in a car or the housing of a microwave oven, while others, e.g. a transistor on a circuit board, are small³. The modern information society arose from, and demands devices that supply fast and easy accessible ways of communication, e.g. computers, cell phones, satellites etc. The needs to make computers and other modern electronic devices more sophisticated create needs to design and with high precision manufacture structures and components on the nanometer scale. Fortunately computers, robots and technological achievements made over the last decades have provided the means to do this. Nanometer sized structures and components are often referred to as nanoelectromechanical systems (NEMS), and are employed in a wide range of fields. In medicine, for example, coated nanometer beams have been used to detect and in some cases also neutralize specific cells, bacteria and viruses⁴⁻⁹. Other examples where NEMS are utilized are: in the manufacture of nanowires, in atomic force microscopy, in high density magnetic recording and in modern electronics such as solar cells, cell phones and computers¹⁰⁻¹⁶. Thus, in everyday life we are surrounded by components that have properties that are determined on the nanometer level.

1.1 Background

In contrast to macrosized structures, the fraction of surface atoms is far from negligible in nanosized structures. The free surfaces break the continuous atomic lattice matrix which results in that the cohesive energy of an atom close to a discontinuity will not be equal to the cohesive energy of a bulk atom. Other examples of discontinuities are grain boundaries, vacancies and interstitials. If the influences from discontinuities become substantial, inaccuracies will appear when applying macroscopic continuum mechanical concepts on the nanoscale. Therefore, today there is a massive interest to find a way to accurately describe the mechanical properties of structures on the nanoscale.

Experiments have shown that the material properties on the nanoscale differ from those on the macroscale. For example, in a study of silver and lead nanowires it was observed that the elastic moduli of the nanowires started to increase as the diameters of the nanowires decreased below 70nm and 100nm, respectively¹⁷. However, for nanocantilevers made of chromium^{18,19} and single crystalline silicon²⁰, the elastic moduli decrease with the sizes of the cantilevers. As the specimen size increases, the discrepancies in material properties diminish, and in an experimental study of single crystalline copper cantilevers with the dimensions $30\ \mu\text{m} \times 3\ \mu\text{m} \times 4\ \mu\text{m}$ ²¹, the measured values of Young's moduli showed good agreement with bulk values.

In agreement with experimental works, papers investigating this issue from a mathematical point of view have shown that the definition of how the dimensions of a nanocrystal are measured affects both Young's modulus^{22,23} and the bending stiffness^{24,25}. The effects of this ambiguity do of course diminish as the size increases²²⁻²⁵. Besides mathematical papers, different simulation tools have been developed and employed to study the mechanical properties of nanostructures. The two most commonly used techniques in computational nanomechanics are molecular statistics (MS) and molecular dynamics (MD)^{26,27}. Papers that utilize MS and MD to study the mechanical properties of nanostructures do in general employ one of the following approaches: tensile, compressive or shear loading²⁸⁻³⁷, beam bending³⁸, or structural frequency response³⁹. As in experiments, computational simulations have shown that the size of a specimen influences its elastic modulus. Furthermore, computer simulations suggest that the specimen size affects the Poisson's ratio^{34-36,40}, the stress- and strain distributions in the vicinity of voids⁴¹⁻⁴³, and that the strain rate affects the elastic moduli of materials^{31,37,44}.

Due to its size, a nanostructure only consists of a few grains. Since grains are anisotropic, the lattice orientations of the grains will strongly influence the mechanical properties of the nanostructure. Besides the mechanical size effects, regarding electrical components, circumstances such as signal delay, crosstalk,

electromigration and stress-induced migration must also be considered as the components are scaled down to the micrometer and nanometer levels⁴⁵. Copper is an element that has low resistivity and can handle high currents; hence, copper is a suitable material for nanoelectronics^{45,46}. In addition, recent studies have shown that copper coating on the silicon anode of a lithium battery not only enhance the storage capacity, but also significantly improve the battery cycle performance⁴⁷⁻⁴⁹. In this dissertation thesis the mechanical properties of highly constrained copper strips and copper coated silicon films similar to the nanostructures studied in⁴⁷⁻⁵¹ are investigated.

Chapter 2

Objectives

The research work presented in this dissertation aims at increasing the understanding and knowledge of copper structures on the nanoscale. To achieve this, two different problem formulations are considered. In the first problem, a highly constrained single crystal copper strip containing a straight through crack shaped void is considered. The strip is simulated with three different geometries and subjected to tensile loading that is parallel to the crack normal. The stress and strains are internally compared and the stress distributions are compared with linear elastic fracture mechanics (LEFM) and finite element (FE) simulations. This problem is discussed in Papers I, II, and III, and the major objectives in these papers are to study how well LEFM and FE apply on the nanoscale and to investigate how different boundary conditions affect the stresses and strains.

The second problem formulation, which is discussed in Papers IV and V, consists of a nanosized silicon film that has a copper coating that is subjected to shear loading. The laminate consists of one silicon crystal and one copper crystal, only. The two crystals are rotated about the interface normals, and the objectives are to investigate how the mechanical properties of the laminate vary with the lattice orientations of the two crystals and to understand the atom movements at the silicon-copper interface and how these movements affect the mechanical properties.

Chapter 3

Atomic simulations

Molecular dynamics (MD) is a computational tool that is frequently used to investigate the properties and responses of materials on the atomic scale. In MD simulations are the motions of atoms or molecules studied. The motions are found by integrating the classical equations of motion for the N particles in the system. In general, after that the N particles have been generated and the temperature T has been set, the system is relaxed, i.e. the particles are free to oscillate and adjust their positions so that the energy is minimized. The relaxation continues until a certain predefined relaxation criterion is met, e.g. the time t is larger than the relaxation time t_{relax} or the system is at equilibrium. Then, after that the relaxation criterion has been met, the load is applied and the numerical data of interest are collected, cf. Figure 3.1^{26,27,52}.

The movements of particles such as atomic nuclei and molecules are described by quantum mechanics and the Schrödinger equation. However, sometimes, depending of the aim, it is not necessary to have a model that takes quantum phenomena into account⁵³. In MD are quantum phenomena not considered and the calculations are reduced to a classical N -body problem. This reduction is justified by two approximations. Firstly, the Born-Oppenheimer approximation which assumes that the motions of atomic nuclei and electrons can be separated, and thus, since an electron roughly is 1800 times lighter than a proton, the electrons will instantly respond to any movements of the atom nuclei. Secondly, the atomic nuclei or molecules are approximated to point particles that are described by Newtonian mechanics^{26,27}. Despite these simplifications the evaluation of the equations of motion of the particles is computationally expensive. Thus, it is essential that the algorithm that integrates the equations of motion is optimized⁵⁴. By truncating the particle interactions with a cut-off radius r_{cut} , the computational costs are reduced^{26,27,53,55}.

Besides effective, the integrating algorithm must also obey the Law of conservation of energy so that the energy in an isolated system does not change²⁶.

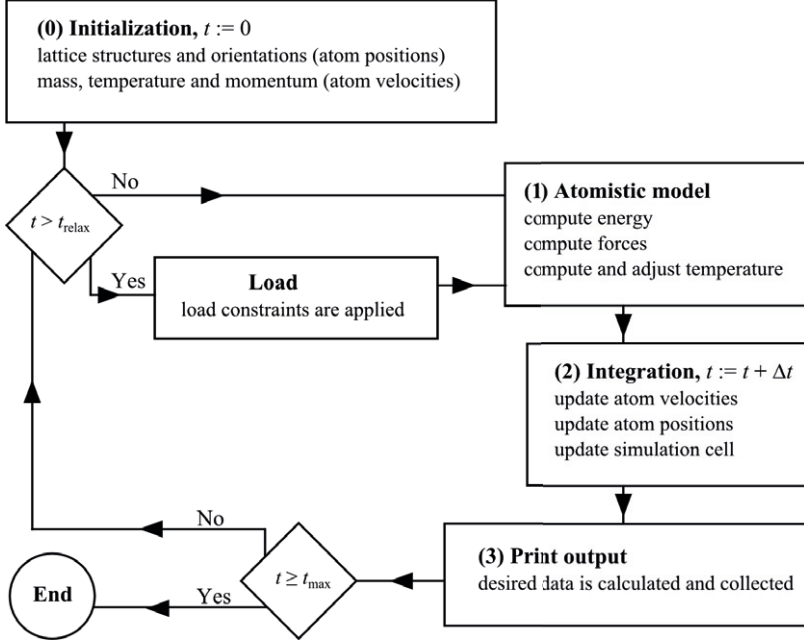


Figure 3.1: Flow chart of the MD simulation process. The sign combination $:=$ symbolizes the assign-command, i.e. $t := t + \Delta t$ means that the value of t increases with Δt .

The problem is that large timesteps are neither able to reproduce the thermal vibrations nor to preserve the energy. The demands are in general fairly met when the timesteps are of the order of $10^{-15}\text{s} = 1\text{fs}$. Thus, all simulations include an economy-accuracy trade-off⁵⁴.

3.1 Governing equations

As implied, in MD simulations are the motions of the atoms governed by Newton's second law:

$$m_i \mathbf{a}_i = \mathbf{f}_i = \sum_{j \neq i} \mathbf{f}_{ij} \quad (3.1)$$

where m_i , \mathbf{a}_i , and \mathbf{f}_i are the mass, acceleration and resulting force of atom i , respectively, and $\mathbf{f}_{ij} = -\mathbf{f}_{ji}$ is the interatomic force between atom i and atom j . The acceleration \mathbf{a}_i is defined as the second time derivative of the position vector \mathbf{r}_i , i.e. $\mathbf{a}_i \equiv \ddot{\mathbf{r}}_i$. The force that one atom exerts on another atom within the truncation radius r_{cut} is described by Eq. (3.2)⁵⁶, with Φ denoting the interatomic potential.

$$\mathbf{f}_{ij} = -\nabla \Phi_{ij}(\mathbf{r}_{ij}) \quad (3.2)$$

In the early 90's Qiu-Dong⁵⁷ presented a series solution that is a general solution to the N -body problem. However, convergence in these series is very slow; hence, this general solution is not employed in numerical works⁵⁸. Instead the equations of motions are solved by integrating Taylor expansions of Eq. (3.1), of the atoms' positions and velocities. A Taylor expansion is a polynomial representation of a function, e.g. $\mathbf{r}(t)$, calculated from the values of the function derivatives $\mathbf{r}^{(n)}(t)$. The Taylor expansion is a direct consequence of the Fundamental theorem of calculus and a repetition of integration by parts:

$$\mathbf{r}(t + \Delta t) = \sum_{n=0}^{\infty} \frac{\mathbf{r}^{(n)}(\Delta t)}{n!} t^n \quad (3.3)$$

In the problem formulation that is considered in Papers I, II, and III, an in-house MD code based on the code found in Rapaport²⁶ is employed. To avoid the need of a velocity estimate, the routine that updates the atom velocities and positions is divided into two parts²⁶; in the first part the atom velocities and positions are updated according to Eqs. (3.4) and (3.5), respectively, and in the second part the atom velocities are updated once more, cf. Eq. (3.6).

$$\mathbf{v}_i(t + \frac{\Delta t}{2}) = \mathbf{v}_i(t) + \frac{\Delta t}{2} \mathbf{a}_i(t) \quad (3.4)$$

$$\mathbf{r}_i(t + \Delta t) = \mathbf{r}_i(t) + \Delta t \cdot \mathbf{v}_i(t + \frac{\Delta t}{2}) \quad (3.5)$$

$$\mathbf{v}_i(t + \Delta t) = \mathbf{v}_i(t + \frac{\Delta t}{2}) + \frac{\Delta t}{2} \mathbf{a}_i(t + \Delta t) \quad (3.6)$$

The temperature T is set by assigning a certain speed to the atoms, cf. Figure 3.1. In MD simulations T is proportional to the average kinetic energy, $\overline{E_k}$:

$$\overline{E_k} = \frac{1}{N} \sum_{i=1}^N \frac{m_i v_i^2}{2} = \frac{\overline{m} \cdot \overline{v^2}}{2} = \frac{3k_B T}{2} \quad (3.7)$$

where, N denotes the number of atoms, v_i is the speed of atom i , k_B denotes the Boltzmann constant, and \overline{m} and $\overline{v^2}$ are the average atom mass and the average of the squares of the speeds, respectively⁵⁹.

3.2 Potentials

There exists a large variety of potentials. In the five papers that are included in this thesis, two different potentials have been employed. In Papers I, II, and III the Lennard-Jones 12-6 potential is employed and in Papers IV and V the Modified embedded atom method potential is employed. The two potentials are briefly discussed below.

3.2.1 The Lennard-Jones potential

The Lennard-Jones (LJ) potential is a pair potential which means that it describes the potential energy of two interacting atoms. Pair potentials are simple and idealized expression that reflects the salient features of real atom interactions. Due to their simple expressions, pair potentials are commonly used in MD simulations^{27,53,54}. Among the pair potentials, the LJ 12-6 potential⁶⁰ is probably the most applied^{26,27}. The LJ 12-6 is presented in Eq. (3.8):

$$\Phi(r_{ij}) = 4\alpha \left[\left(\frac{\beta}{r_{ij}} \right)^{12} - \left(\frac{\beta}{r_{ij}} \right)^6 \right] \quad (3.8)$$

where Φ is the potential energy, r_{ij} is the interatomic distance between atom i and atom j , and α and β are the depth of the potential well and the interatomic distance at which Φ equals zero, respectively. Since it has been shown that the long ranged attracting force varies with r^{-7} , the r^{-6} -term in the LJ expression is rooted in physics. The short range repulsive force is not as essential as the long range force. Therefore, due to convenience, the exponent in the repulsive term is set to 12^{59,60}.

The drawbacks with pair potentials are that pair potentials do not account for any directional nature of atomic bonds and have no environmental dependence^{27,61}. In addition, pair potentials satisfy the Cauchy stress relation, $C_{12} = C_{44}$, where C_{ij} denotes the elastic components, something which in general is not true for solid cubic lattice metals^{62,63}. Even so, pair potentials are commonly employed when simulating metals such as copper, in which the cohesion is provided by s or p electrons²⁷.

3.2.2 The Modified embedded atom method

The Modified embedded atom method (MEAM)^{64,65} is an extension of the Embedded atom method (EAM) which is a semi-empirical many-body potential. Many-body potentials have one pair potential term and one many-body term. The many-body term describes the interaction between the atoms and the background electron density^{66,67}. In contrast to the EAM potential, the MEAM potential can handle angular dependencies. Thus, the MEAM potential is able to include bond-bending forces; something that is necessary to describe semiconductors^{64,68}. In the EAM and MEAM potentials, the total energy, E , is described by Eqs. (3.9) and (3.10):

$$E = \sum_i E_i \quad (3.9)$$

$$E_i = F_i(\bar{\rho}_i) + \frac{1}{2} \sum_{j \neq i} \Phi(r_{ij}) \quad (3.10)$$

where E_i is the energy of atom i , F_i is the embedding function representing the energy that a cation of atom i 's type gets when it is surrounded by the background electron density at the position of atom i , $\bar{\rho}_i$ is the background electron density at the position of atom i , and Φ is the pair potential that acts between atom i and atom j . The extension that enables the MEAM potential to include angular dependencies is added into the embedding function^{68,69}. Both the EAM and MEAM potentials are frequently used in MD simulations⁶⁹.

3.3 Periodic boundary conditions

Due to computational costs, the number of atoms, N , is limited in a MD simulation. The N -limitations that modern super computers offer are negligible in comparison with the number of atoms in a specimen that can be seen by the naked eye. Consequently, MD simulations performed with free boundaries are significantly influenced by the surfaces. Unless the aim is to study the properties near the surfaces, the influences from the free surfaces have to be eliminated so that the simulation captures the nature of a large specimen. By imposing periodic boundary conditions (PBC) the surface influences can be removed. PBC mimics the presence of an infinite bulk by enclosing all N particles within a box and then placing imaged copies of this box edge to edge to the original one, cf. Figure 3.2. In addition, in PBC, if an atom leaves the simulation box it reenters the simulation box on the other side with the same velocity. To prevent that atoms interact with themselves the distance between two parallel sides of the simulation box must be at least $2r_{\text{cut}}$ ^{26,27,52,54}.

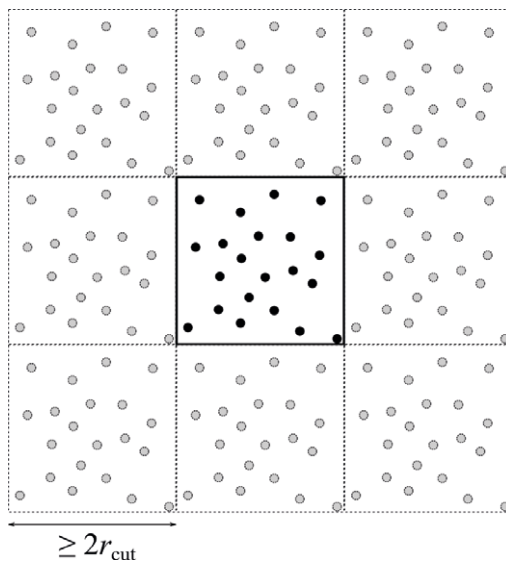


Figure 3.2: Schematic illustration of PBC. The solid black box and the black dots illustrate the simulation box and its atoms. The dashed boxes containing grey dots represent the imaged copies of the simulation box and its atoms.

Chapter 4

Problem formulations

In this Chapter, the two problem formulations are presented. To be able to describe the two problems, some basic material science concepts are needed. These concepts are presented in section 4.1. The problem formulation that is under consideration in Papers I, II, and III is found in section 4.2 and the problem formulation that is under consideration in Papers IV and V is described in section 4.3.

4.1 Lattice structure and anisotropy in copper and silicon

Metals and semiconductors are in general crystalline which means that the atoms are arranged in highly ordered matrices. The particle arrangement that is repeated within a matrix is called lattice structure and the smallest entity that the matrix can be divided into without losing the lattice structure is called a unit cell^{2,3}. Up to its melting point, the only stable lattice structure for copper is the faced-center cubic (FCC) lattice structure⁷⁰. The FCC unit cell is a cubic entity with one atom in each corner and one atom centered on each of the six surfaces, cf. Figure 4.1a. In silicon the atoms are generally arranged in the cubic diamond lattice structure cf. Figure 4.2a^{69,71}. The cubic diamond lattice structure is similar to the FCC lattice structure and in both structures are the $\langle 110 \rangle$ -lattice directions the most closely packed directions and thus the directions in which slip generally occur, cf. Figures 4.1b-e and Figures 4.2b-e.

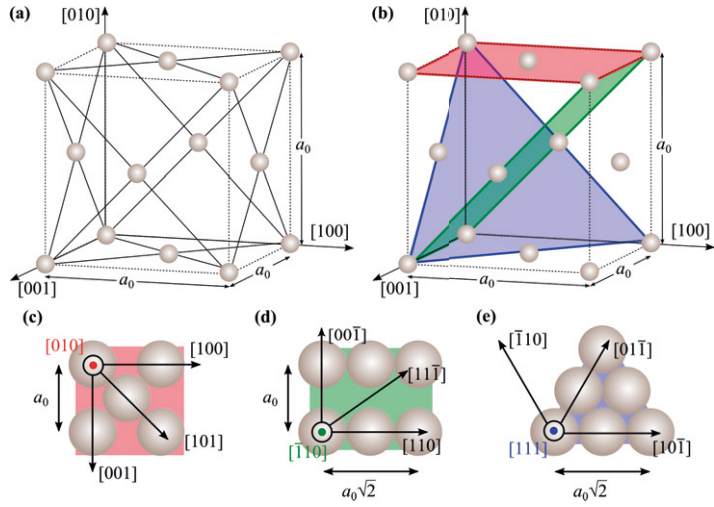


Figure 4.1: The FCC unit cell. (a) is a schematic illustration of the FCC unit cell. In (b) the (010) -, $(\bar{1}10)$ -, and (111) -planes are drawn into the unit cell and colored with red, green and blue, respectively. Figures (c), (d), and (e) are scale illustrations of the three planes represented in (b). a_0 denotes the lattice parameter.

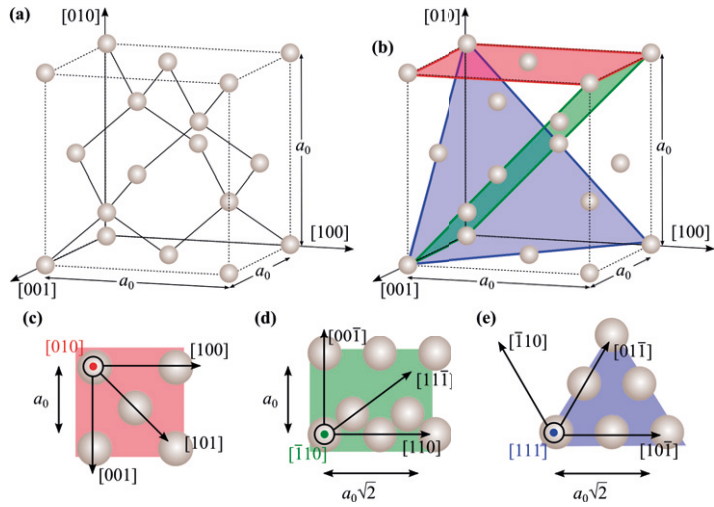


Figure 4.2: The cubic diamond unit cell. (a) is a schematic illustration of the diamond unit cell. In (b) the (010) -, $(\bar{1}10)$ -, and (111) -planes are drawn into the unit cell and colored with red, green and blue, respectively. Figures (c), (d), and (e) are scale illustrations of the three planes represented in (b). a_0 denotes the lattice parameter.

The interatomic spacing affects properties such as the electrical conductivity, the thermal conductivity, the Young’s modulus, and the fracture toughness^{2,3,72}. As a result, these properties have different values in different lattice directions, cf. Figures 4.1c-e and Figures 4.2c-e, and this directional dependency is called anisotropy. In Table 4.1 values of Young’s modulus in three lattice directions are listed for the elements copper and silicon.

Table 4.1: Young’s modulus for copper and silicon in three different lattice directions.

| Element | Young’s modulus (GPa) | | |
|---------|-----------------------|--------------------|--------------------|
| | [100] | [110] | [111] |
| Copper | 66.7 ^a | 130.3 ^a | 191.1 ^a |
| Silicon | 130 ^{b,c} | 170 ^{b,c} | 189 ^c |

^aRef. [2].

^bRef. [73].

^cRef. [74].

4.2 The flawed copper strip

The flawed copper strip consists of a single crystal FCC copper strip. The strip has the shape of a cuboid and the strip width, depth and height measures are $2W$, $2d$, and $2h$, respectively. The strip edges are parallel to the \boldsymbol{x} -, \boldsymbol{y} -, and \boldsymbol{z} -directions which coincide with the [100]-, [010]-, and [001]-lattice directions, respectively, cf. Figure 4.3. The height is divided into three blocks: one of height $2h^*$ and two of height $3a_0$, where a_0 is the lattice parameter. The two latter blocks, one placed at the bottom and one placed at the top, are marked with dashed lines in Figure 4.3 and are from here on referred to as the bottom and top blocks. With the purpose to mimic a centrally placed crack, a straight through void is created by removing atoms at the center of the strip. For simplicity, the void is shaped as a cuboid with the dimensions $2a \times 2d \times 2b$, similar to the voids in Dienes and Paskin⁷⁵ and Mayer and Krasnikov⁷⁶.

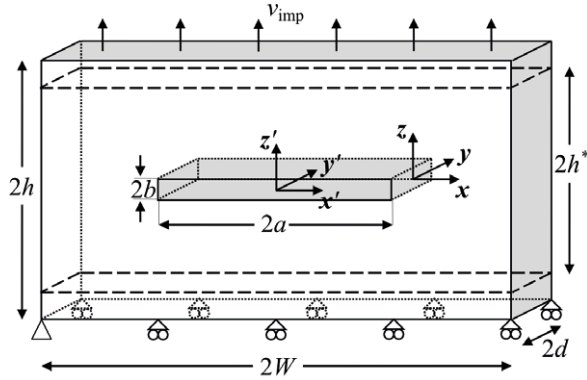


Figure 4.3: Schematic illustration of the flawed copper strip.

All atoms in the bottom atom layer are fixed in the z -direction and the atom in the leftmost corner is fixed in the x - and y -directions as well. Initially, during the relaxation, the rest of the atoms in the bottom block are forced to move so that the atom layers are kept plane and the interlayer distances are kept constant. The same constraint, i.e., keeping the interlayer distance fixed, is also applied on all atoms in the top block. During the loading phase, all atoms in the bottom block are prevented from moving in the z -direction and a displacement controlled tensile load is imposed by forcing all atoms in the top block to move with a constant speed in the positive z -direction, v_{imp} .

The flawed strip is simulated with three different geometries: G1, G2, and G3. In G1, PBC are applied in the x - and y -directions while the dimension in z varies. Thus each strip simulated with the G1 geometry can be seen as an infinite film. Considering G2, PBC is applied in the y -direction while the width $2W = 200a_0$ and the height $2h^*$ varies. Hence G2 may be seen as a hollow infinite rod. In G3 PBC are applied in x , varies in y and measures $2h^* = 20a_0$ in z ; thus, G3 can be seen as an infinite rod, cf. Table 4.2.

Table 4.2: Geometry G1, G2, and G3. For coordinate system, cf. Figure 4.3.

| Geometry | G1 | G2 | G3 |
|--------------------------|---------------------|---------------------|---------------------|
| Dimension in x | Periodic | 723Å | Periodic |
| Dimension in y | Periodic | Periodic | Variable |
| Dimension in z | Variable | Variable | 72.3Å |
| Void size $2a \times 2b$ | 362Å \times 7.23Å | 362Å \times 7.23Å | 362Å \times 7.23Å |

The simulations are performed in an in-house MD program developed by the author. The source code is written in C99 and based on the open source code provided by Rapaport²⁶. The strips are simulated at the temperature

$T = 1\text{K}$ and the Lennard-Jones potential is employed to describe the atomic interactions. All simulations start with a relaxation whose length increases with N . Furthermore v_{imp} is set so that the strain rate $\dot{\epsilon} = 5 \cdot 10^8 \text{s}^{-1}$ in all simulations. The common parameters that are essential for the simulations and the material properties are listed in Table 4.3.

Table 4.3: Simulation and material related parameters.

| | |
|--|----------------|
| Lattice constant a_0 (\AA) | 3.6151 |
| Potential well depth α (eV) | 0.1515 |
| Distance for zero potential β (\AA) | 2.338 |
| Cut-off radius r_{cut} (\AA) | 6.406 |
| Strain rate $\dot{\epsilon}$ (s^{-1}) | $5 \cdot 10^8$ |
| Temperature T ($^\circ\text{K}$) | 1.0 |

4.3 The copper coated silicon film

The copper coated silicon film consists of two single crystal films; one of FCC copper and one of cubic diamond silicon, cf. Figure 4.4. The films are quadratic and have a side length equal to about 217\AA . This value is chosen since 217\AA is the approximate length of 60 and 40 unit cells in the $\langle 100 \rangle$ -lattice directions for copper and silicon, respectively. The thicknesses, i.e. the heights, of the silicon and copper films are h_{Si} and h_{Cu} , respectively. To minimize the computational cost but still ensure that the silicon atoms at the bottom and the copper atoms at the top do not directly influence the interface and to ensure that the copper coating can deform continuously, h_{Si} and h_{Cu} are set to about 28.5\AA and 42.5\AA , respectively, cf. Figure 4.4.

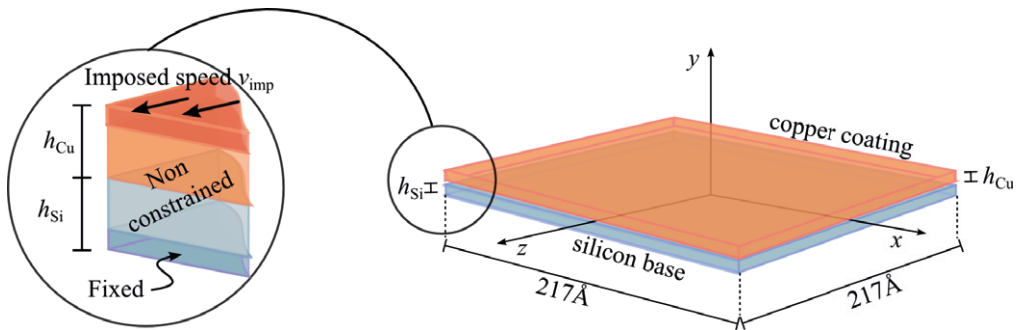


Figure 4.4: Schematic illustration of the simulated films. The atoms within the dark copper colored volume and the atoms within the dark blue colored volume according to the zoom-in to the left, hold the boundary constraints.

The films are simulated in the freeware LAMMPS⁷⁷ and MEAM potential is employed to describe atomic interactions. The employed potential and the lat-

tice parameters for silicon and copper, a_{Si} and a_{Cu} respectively, are taken from Jelinek *et al.*⁶⁹. The coated film is simulated with many different combinations of lattice orientations. Seventeen different lattice orientations combinations are considered in Paper IV, while Paper V only considers two. However, the two lattice orientations combinations in Paper V are rotated about the \mathbf{y} -axis, cf. Figure 4.4, so that the shear load is applied in four and six different lattice orientations, respectively; hence, in Paper V, ten different load cases are considered.

The coated film is simulated at a temperature $T = 300^\circ\text{K}$ and a NVT integrator with a Nosé-Hoover thermostat²⁷ is employed. Each simulation starts with a relaxation that lasts for 10,000 timesteps which corresponds to 10ps. During the loading phase all atoms in the top two Cu atom layers are forced to move with a constant speed $v_{\text{imp}} = 0.02172\text{\AA}/\text{ps}$ in the \mathbf{z} -direction. The constant shearing speed causes a displacement controlled load with a constant strain rate $\dot{\epsilon} = 10^8\text{s}^{-1}$. A final shear of 5% in the \mathbf{z} -direction is achieved by integrating the system for 500,000 timesteps. Throughout the simulations the two bottom silicon atomic layers are fixed in the \mathbf{x} -, \mathbf{y} -, and \mathbf{z} -directions, cf. Figure 4.4.

Chapter 5

Results

In Papers I, II, and III the flawed copper strip, cf. section 4.2, is considered, and the papers focus on describing the stresses and strains in the vicinity of the crack shaped void. Papers IV and V consider the copper coated silicon films, cf. section 4.3, and the anisotropy in shearing is studied. In section 5.1 the main results from Papers I, II, and III are presented and section 5.2 contains the main results from Papers IV and V.

5.1 Main results in Papers I, II, and III

In Paper I it was shown that elastic properties of the strip varied with the strip size and geometry. It was also observed that MD, under the considered circumstances, generates peanut shaped stress distributions, cf. Figure 5.1. Considering the shapes, these stress distributions show good agreement with the stress distributions generated by FE and are similar to the stress distribution that LEFM predicts for an infinitesimal crack. If the distributions in Figure 5.1 are studied carefully, it is observed that MD and FE predict differently when it comes to the location of the highest tensile stresses and how the tensile stress behave ahead of the void tip. This becomes even clearer when the curves in Figure 5.2 are studied. The reason why the MD simulations generate the highest tensile stresses a few atoms ahead of the void tip instead of at the void tip is the fact that the atoms near the void are lacking neighbors. Since no dislocation nucleations or bond breakages are observed in Paper I, it is concluded that lattice defects such as voids affect the elastic response of a crystal.

Studying Figures 5.1a and d it is seen that the void tips have been blunted. In addition, Figure 5.1b reveals a small gap indicating a large strain. Furthermore, in Figure 5.2 it is seen that MD predicts higher stresses than FE in short intervals ahead of the void tips. These observations indicate that the deformations are

elasto-plastic rather than purely elastic. However, as mentioned, no dislocation nucleations or bond breakages are observed and since the LJ potential is capable of reproducing these phenomena, cf.^{78,79}, the LJ potential is most likely not a source of error. In addition, assuming plastic deformation in G1, then the maximum stress in G1 corresponds to the yield strength, σ_{YS} , cf.⁸⁰. However, since the maximum stress in G2 is higher than the maximum stress in G1, the maximum stress in G1 cannot be σ_{YS} . Thus, the blunting of the void tips are elastic and the conclusion about that lattice defects such as voids affect the elastic response of a crystal must be correct.

In Paper I it is also shown that the similarities between MD and FE decrease with the specimen size and that the tensile stresses increase with the dimension parallel to the loading direction and that the larger the strip size, the more extended stress fields.

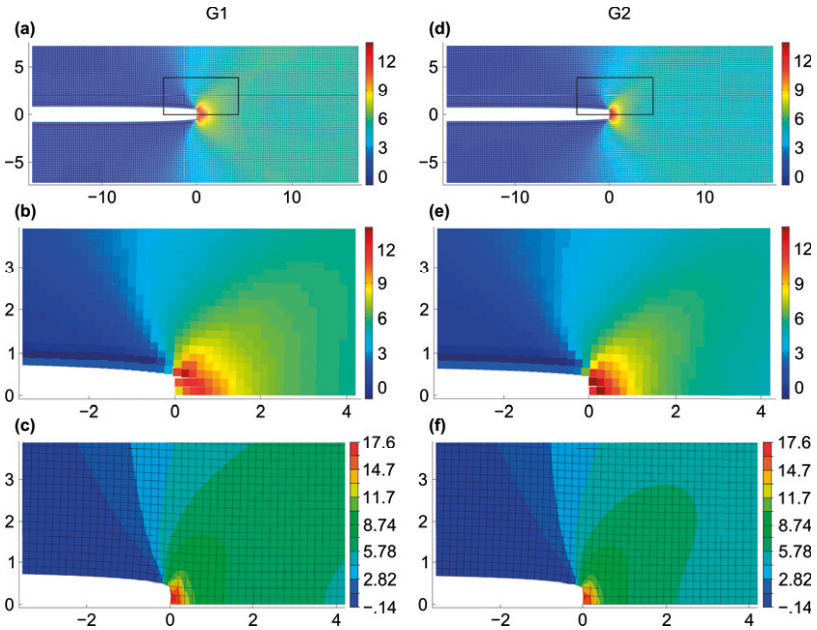


Figure 5.1: Stress field distributions generated from MD and FE simulations for the geometries G1 (left-hand side) and G2 (right-hand side) for $2h^* = 40a_0$. (a) and (d) are MD simulations and the black frames mark the zoomed in areas shown in (b) and (e), respectively. (c) and (f) are FE simulations. The color bars are given in GPa and the abscissas and ordinates show the x - and z -coordinates in nm.

Papers II and III focus on geometry G3. In Paper II it is shown that under uniaxial tensile strain, MD is in agreement with the theory and generates higher stresses when plane strain applies as compared to when plane stress applies. It is also observed that the tensile stress decreases faster with the distance to the void tip in regions where plane strain reigns than in regions where plane stress reigns. This is explained by the stresses that are built into the system when the loading starts, cf. Figures 5.3a and b. In Paper II it is observed that the deviations between MD and FE simulations seem to decrease as the depth $2d$ and/or the tensile strain increase. However, for strips with smaller depths the deviations increase with the tensile strain, cf. Figure 5.3.

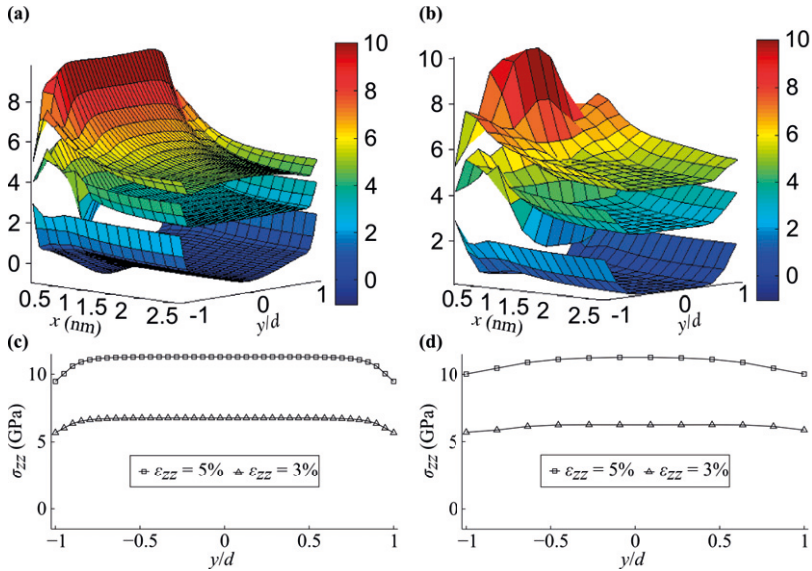


Figure 5.3: Stress distributions ahead of crack for $2d = 20a_0$ (a) and (c) and for $2d = 6a_0$ (b) and (d). In (a) and (b) the color bars and the vertical axes show σ_{zz} in GPa. The three surface plots seen in the two figures represent the stress distributions at the tensile strain $\epsilon_{zz} = 0\%$, $\epsilon_{zz} = 3\%$ and $\epsilon_{zz} = 5\%$. (c) and (d) are taken from FE simulations and show σ_{zz} at the second atom ahead of the void tip.

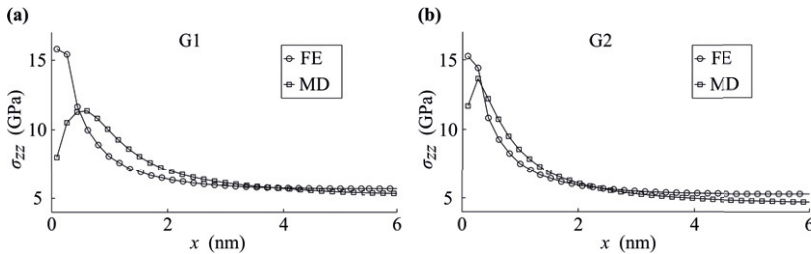


Figure 5.2: Tensile stress versus distance at $y, z \approx 0$, $\sigma_{zz}(x, 0, 0)$ for simulations with $2h^* = 40a_0$.

When the strains are studied in Paper III it is observed that, when $2d = 6a_0$, from the fourth atom plane ahead of the void tip and onward, the minimum tensile stresses are found at $y = 0$. Considering the strips with $2d = 10a_0$, $20a_0$ and $30a_0$, if the surface layer and the two following layers are excluded, the strips agree with continuum theory and have the maximum tensile stresses along the y -axis. Hence it is concluded that strips that have a dimension of $6a_0$ in a direction orthogonal to the loading direction never experience plane strain. Moreover, the results in Paper III show that the planes with a normal parallel to the crack direction bend towards the void center, cf. Figure 5.4, and that the dispersions of the atom positions in the surface layers are larger near the void tip than far away, cf. Figure 5.5. Despite this observation, the free surface effects are more prominent a few planes ahead of the void tip than at the void tip, cf. Figure 5.3.

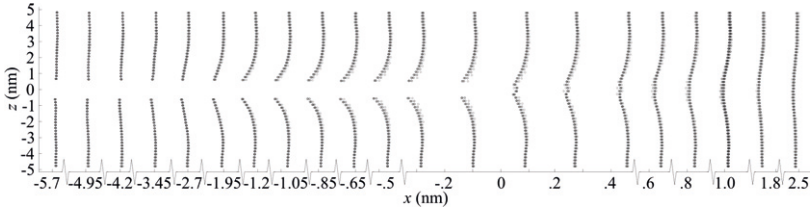


Figure 5.4: Some (100)-planes near the void tip when $2d = 6a_0$ at a tensile strain $\epsilon_{zz} = 5\%$. Note that the abscissas have several interruptions.

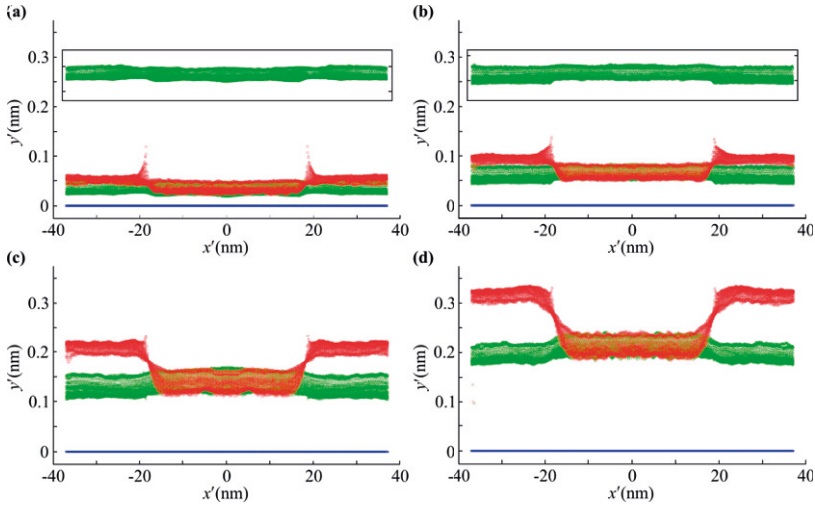


Figure 5.5: Atom positions in the primed coordinate system (cf. Figure 4.3) for the surface (010)-plane. Blue circles: initial configurations; green circles: after relaxation, i.e. $\epsilon_{zz} = 0\%$; red circles: $\epsilon_{zz} = 5\%$. (a) $2d = 6a_0$, (b) $2d = 10a_0$, (c) $2d = 20a_0$, and (d) $2d = 30a_0$. The framed green circles in (a) and (b) show the relaxed configurations and the markings on the frames belong to $y' = 0$, $y' = 0.5$ and $y' = 0.5$, $y' = 1.0$ for (a) and (b), respectively.

5.2 Main results in Papers IV and V

In Paper IV it is observed that the Cu coating starts to slide upon the Si film after a certain displacement threshold, which is specific for each lattice orientation combination. Despite that the Cu coating slides, deformations are observed in the vicinity of the interface at the front and at the rear of the laminate. Considering lattice orientation combinations with force-displacement curves (FDC) that oscillates periodically, sliding occurs within the intervals in which the derivatives of the FDCs are strictly negative. Furthermore, the initiation of the sliding breaks the linear behavior and it is concluded that the relocations, i.e. the movements to adjacent but distinctly new positions, of Cu atoms at the interface affect the mechanical properties, cf. Figure 5.6.

When the shapes of the FDCs are studied, none of the trends observed suggest that the shape of the FDC is determined by the lattice orientation of only one of the elements. The observations do rather imply that the shape of the FDC is determined by the atom position agreement, i.e. the accordance in atomic positions, at the Si-Cu interface. Moreover, it is found that the oscillation period length depend on the linear atomic density in the direction of the total displacements and the angle between the load direction and the direction of the total displacements.

The mechanical properties vary widely with the lattice orientation combinations. Among the 17 studied combinations, cf. Table 1 in Paper IV, the design that is the most suitable for the case where a structure is exposed to a shear force and no atom relocations are allowed to take place is the design where the Si and Cu crystals are orientated in the same way and have the interface normal and the shear load applied in $\langle 100 \rangle$ -directions. However, under the same circumstances but instead of force, a displacement is applied, the most favorable design is when the Si and Cu crystals are orientated in the same way, have the interface normal in the $[\bar{1}10]$ -direction and have displacements applied in the $[001]$ -direction.

In Paper V it is concluded that the oscillations in the FDCs are explained by that, when the Cu coating moves over the Si film, the atom position agreements at the interface are periodically relatively good and periodically bad. Among the ten load cases that are considered in Paper V it is observed that some load cases have sinusoidal wave-shaped FDCs, some have sawtooth wave-shaped FDCs, and some have FDCs that are something in-between, cf. Figure 5.7. It is found that the shape of the FDC is determined by how the Cu atoms at the Si-Cu interface relocate which, in turn, are explained by the lattice agreement, the interface normal, and the angle between the load-direction and the slip direction that is the most parallel to the load-direction, β_{slip} .

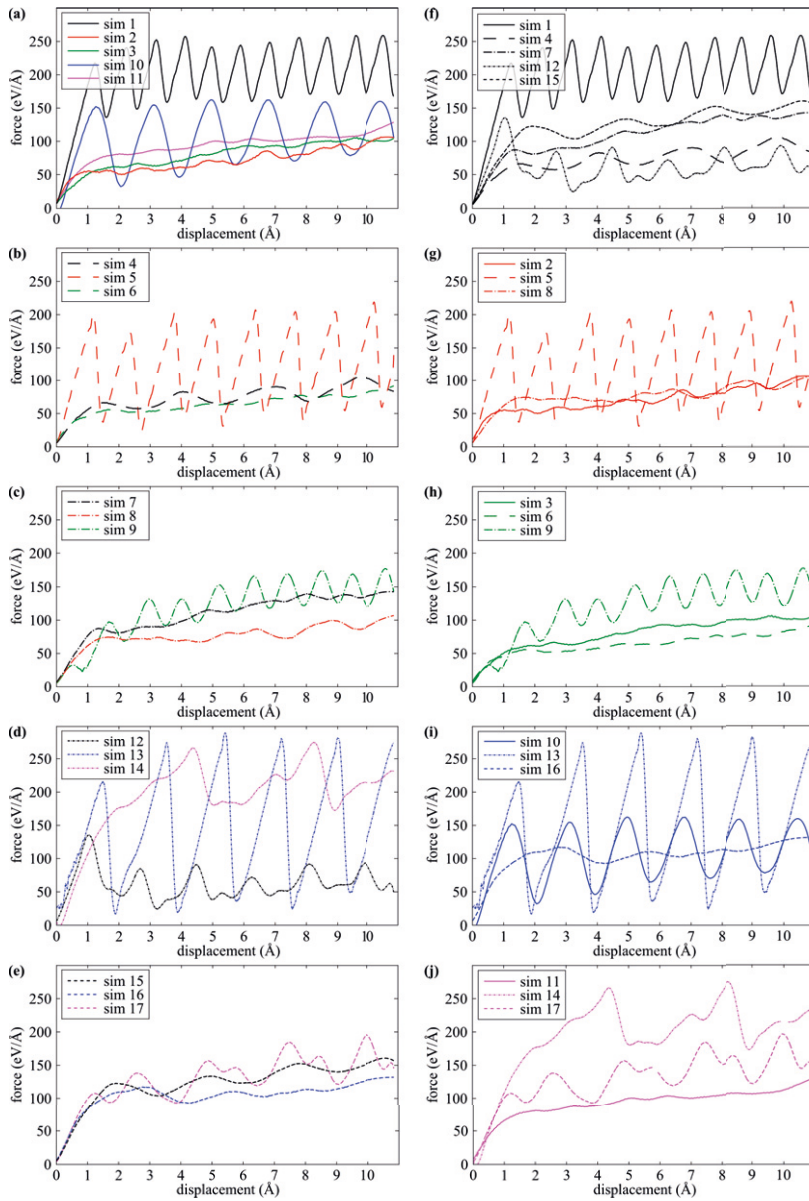


Figure 5.6: Force-displacement curves; the abscissas show the imposed shear displacement and the vertical axes show the z -component of the internal force of the structure. The line-type identifies the orientation of the Cu coating and the color identifies the orientation of the Si film, cf. Tables 1 and 3 in Paper IV.

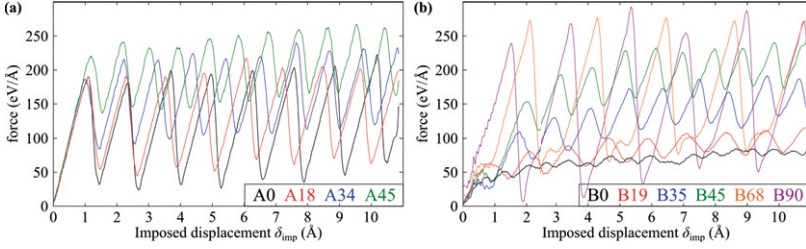


Figure 5.7: Force-displacement curves; the abscissas show the imposed shear displacement and the vertical axes show the z -component of the internal force of the structure, cf. Table 1 in Paper V.

When the Si and Cu matrices are orientated in the same way and when none of the interface planes belong to the plane family with the most densely packed planes, i.e. the $\langle 111 \rangle$ -planes, the Si and Cu atoms are able to adjust their positions so that the interface consists of repeated atom formations with spacing in-between. Thus, all relocations that occur in each load case are similar, and, therefore, the mechanical properties and the shapes of the FDCs can be explained by studying the typical relocation for each load case.

In simulation group B, i.e. the simulations that have the interface normal in the $[110]$ -lattice direction, cf. Table 1 in Paper V, two types of relocations are observed: crossing and parallel movement. As the names imply crossing is when the Cu atom moves orthogonal to the repeated Si atom arrangement, and parallel movement is when the Cu atom moves parallel to the repeated Si atom arrangement along a slip-direction, cf. Figure 5.8. For the considered load cases, crossing only occurs when $\beta_{\text{slip}} > 45^\circ$ and lead to large force oscillation amplitudes and large relocation leaps which result in sawtooth wave-shaped FDCs, cf.

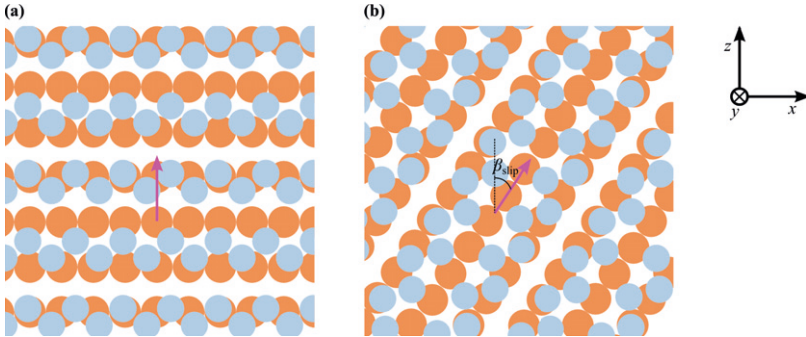


Figure 5.8: The two general types of relocations in simulation group B. (a) crossing - the Cu atoms move across (not necessarily perpendicular to) the Si atom periodic arrangements and (b) parallel movement - the Cu atoms move parallel to the Si atom arrangements.

A0 and B90 in Figure 5.7. When the angle β_{slip} is small all atom movements are parallel and continuous, and the force that tries to prevent the shearing, i.e. f_z , is small and sinusoidal wave-shaped, cf. B0 and B19 in Figure 5.7. As β_{slip} increases, the applied load forces the Cu atoms to move closer to the Si atoms. This increases the atomic interactions which result in a larger force offset, f_{offset} , about which the force f_z oscillates. Since the ability to absorb strain energy mainly is determined by f_{offset} , a structure's ability to absorb strain energy is maximum when f_{offset} is maximal, which occurs when $\beta_{\text{slip}} = 45^\circ$. Furthermore, as the angle β_{slip} increases the movements in the load direction become less continuous and relocation leaps start to appear. Together with the increased atomic interactions, these relocation leaps result in larger oscillation amplitudes, cf. Figure 5.7 and Figure 5.9.

In simulation group A, i.e. the simulations that have the interface normal in the [010]-direction, cf. Table 1 in Paper V, only one type of relocation is observed. Here all relocations appear in the [101]-direction, which is a slip direction. As in simulation group B, the angle β_{slip} strongly affects the mechanical properties and as β_{slip} increases the ability to absorb strain energy increases. However, in contrast to simulation group B, in simulation group A the force oscillation amplitude decreases when β_{slip} increases. This is explained by the fact that a relocation in simulation group A can be described as a Cu atom passing through a gate consisting of two Si atoms, and as β_{slip} increases, the maximum magnitude of the counteracting force decreases, cf. Figure 5.10. The force distribution, however, expands which results in more continuous peaks, cf. Figure 5.7 and Figure 5.11.

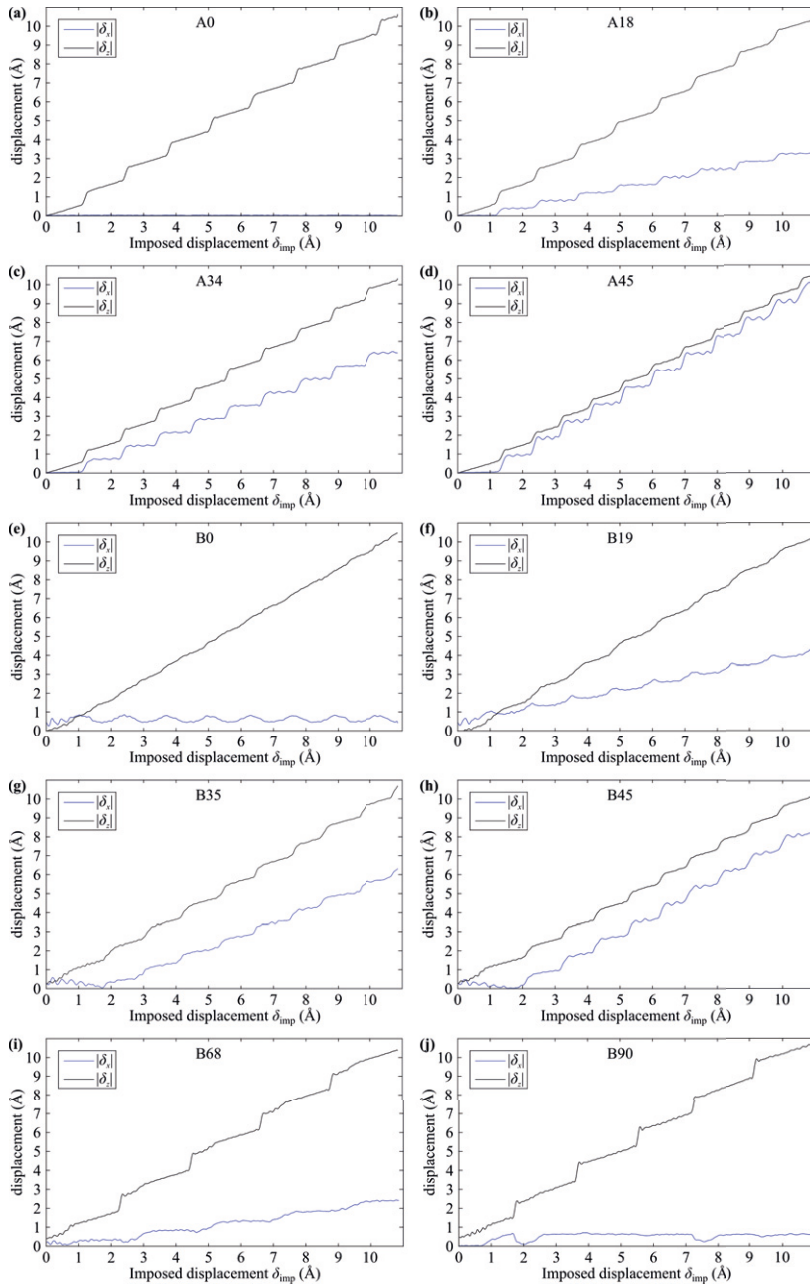


Figure 5.9: Displacement-displacement curves; the abscissas show the imposed shear displacement and the vertical axes show the displacements in x and z .

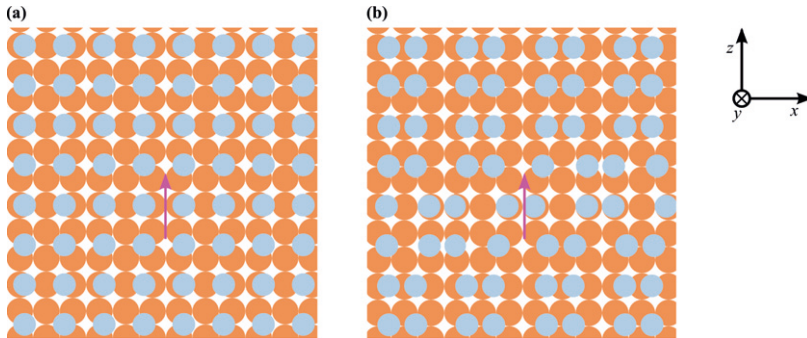


Figure 5.10: Visualization of how the Cu atoms in simulation group A relocate. (a) is a screen taken at $t = 0$ ns and (b) is a screen taken at $t = 6.4$ ns. Note that the Si atoms in the $[\bar{1}01]$ -direction rearrange so that the direction reminds of a $\langle 111 \rangle$ -direction.

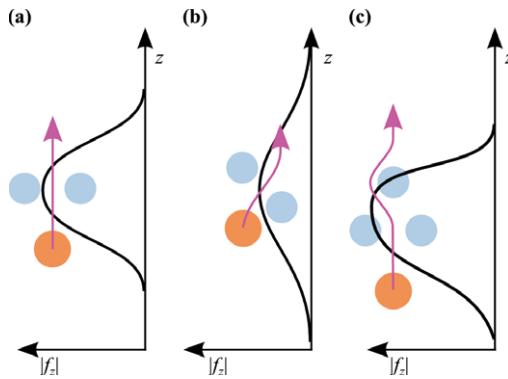


Figure 5.11: Schematic illustration of the force magnitude when: (a) - a Cu atom passes a pair of Si atoms that form a gate, (b) - a Cu atom passing a gate when $\beta_{\text{slip}} = 45^\circ$, and (c) - a Cu atom moves up upon three Si atoms as in simulation B90, cf. Paper IV.

Chapter 6

Conclusions

The work presented in this thesis is based on five papers (I, II, III, IV, and V) that investigate nanosized Cu structures by employing molecular dynamic simulations. In Papers I, II, and III a highly constrained Cu strip that contains a straight through crack shaped void was considered. The strip was simulated with three different geometries which all were subjected to tensile displacement controlled loading, and the stress- and strain distributions in the vicinities of crack shaped voids were studied. Papers IV and V considered a Cu coated thin Si film that was subjected to displacement controlled shear loading. The papers aimed to investigate the variations in mechanical properties among different lattice orientation combinations and the shear anisotropy.

Considering the shape of the stress field distributions ahead of the crack shaped void, the finite element simulations and molecular dynamics simulations showed good agreement. However, the two methods predicted differently for the location of the highest stresses. Also, finite element and molecular dynamics generated different tensile stress decays ahead of the void tips. Thus it was concluded the finite element method cannot be used to model nanosized structures.

For the simulations with large measures in the load direction, molecular dynamics showed that the highest tensile stresses is not found directly at void tip, but rather a few atoms into the specimen. Also, large tensile stresses were found near the singular points at the void tip. For the simulations with small measures in the load direction, however, the highest tensile stresses were either found at the void tip or close to the singular points at the void corners. The different locations can maybe be explained as a combination of the cross-like stress field distribution seen in Fig. 3c in Paper III and the conclusions that the tensile stress increases with dimension parallel to the load direction and that the larger the strip size, the more extended stress field distributions.

It was also concluded that lattice defects such as voids affect the elastic

response of a crystal and that strips that have a dimension of $6a_0$ in a direction orthogonal to the loading direction never experience plane strain.

For the Cu coated Si film, it was concluded that when a crystal is sheared upon another, the shape of the force-displacement curve is determined by the atom position agreement i.e., the accordance in atomic positions, at the interface. In addition, together with the interface normals and the angle between the load direction and the slip direction that is the most parallel to the load direction, β_{slip} , the atom position agreement determines how an atom at the interface relocate, i.e. move to adjacent but distinctly new position. Considering the relocation it was concluded that the larger relocation movements, the more sawtooth wave-shaped force-displacement curve. However, if the relocation movements are small, the force-displacement curve become sinusoidally wave-shaped or continuous in another way. Moreover, the relocations affect the mechanical properties heavily, and in some simulations the relocation of Cu atoms at the Si-Cu interface ends the linear mechanical behavior.

Furthermore it was found that if a copper coated silicon film is exposed to shear forces and relocations at the interface are not allowed to occur, both the Si film and the Cu coating shall be orientated so that the free surface normals and the applied shear load coincide with a $\langle 100 \rangle$ -direction. However, if the film is exposed to shear displacements, the most favorable design among the tested in Papers IV and V, is the one that has the $[\bar{1}10]$ -direction defining the interface normal and the load applied in the $[001]$ -direction, cf. Table 1 in Paper IV.

The oscillations in the force-displacement curves arise because the atom position agreement varies as the Cu coating shears upon the Si film. In the force-displacement curve belonging to the load case in which $\beta_{\text{slip}} = 90^\circ$, small bulges where observed. These bulges coincide with displacements orthogonal to the load direction. By studying the atom movements and forces it was concluded that the orthogonal movements occur due to an unstable atom position agreement between the two crystals. As a result of the orthogonal displacements, less force is needed to shear the coating upon the film.

Finally, it was also concluded that the ability of a structure to absorb strain energy increases with the angle β_{slip} and is maximum when $\beta_{\text{slip}} = 45^\circ$.

References

- [1] C. Ferguson, “Historical introduction to the development of material science and engineering as a teaching discipline,” available from the UKCME at <http://www.materials.ac.uk/pub/Materials-History-Intro.pdf> (2006).
- [2] W. D. Callister and D. G. Rethwisch, *Fundamentals of materials science and engineering*, Vol. 471660817 (Wiley, 2013).
- [3] R. E. Smallman and R. J. Bishop, *Modern physical metallurgy and materials engineering* (Butterworth-Heinemann, 1999).
- [4] B. Ilic, D. Czaplewski, H. G. Craighead, P. Neuzil, C. Campagnolo, and C. Batt, “Mechanical resonant immunospecific biological detector,” *Applied Physics Letters* **77**, 450–452 (2000).
- [5] B. Ilic, H. Craighead, S. Krylov, W. Senaratne, C. Ober, and P. Neuzil, “Attogram detection using nanoelectromechanical oscillators,” *Journal of Applied Physics* **95**, 3694–3703 (2004).
- [6] B. Ilic, Y. Yang, and H. G. Craighead, “Virus detection using nanoelectromechanical devices,” *Applied Physics Letters* **85**, 2604–2606 (2004).
- [7] D. Reich, M. Tanase, A. Hultgren, L. Bauer, C. Chen, and G. Meyer, “Biological applications of multifunctional magnetic nanowires,” *Journal of Applied Physics* **93**, 7275–7280 (2003).
- [8] A. Hultgren, M. Tanase, C. S. Chen, G. J. Meyer, and D. H. Reich, “Cell manipulation using magnetic nanowires,” *Journal of applied physics* **93**, 7554–7556 (2003).
- [9] A. Gupta, D. Akin, and R. Bashir, “Single virus particle mass detection using microresonators with nanoscale thickness,” *Applied Physics Letters* **84**, 1976–1978 (2004).

- [10] D. Sellmyer, M. Zheng, and R. Skomski, “Magnetism of fe, co and ni nanowires in self-assembled arrays,” *Journal of Physics: Condensed Matter* **13**, R433 (2001).
- [11] J. Wang, X. Zhou, Q. Liu, D. Xue, F. Li, B. Li, H. Kunkel, and G. Williams, “Magnetic texture in iron nanowire arrays,” *Nanotechnology* **15**, 485 (2004).
- [12] M. B. Viani, T. E. Schäffer, A. Chand, M. Rief, H. E. Gaub, and P. K. Hansma, “Small cantilevers for force spectroscopy of single molecules,” *Journal of Applied Physics* **86**, 2258–2262 (1999).
- [13] T. Stowe, K. Yasumura, T. Kenny, D. Botkin, K. Wago, and D. Rugar, “Attonewton force detection using ultrathin silicon cantilevers,” *Applied Physics Letters* **71**, 288–290 (1997).
- [14] X. Zhang, G. Wen, Y. Chan, R. Zheng, X. Zhang, and N. Wang, “Fabrication and magnetic properties of ultrathin fe nanowire arrays,” *Applied physics letters* **83**, 3341–3343 (2003).
- [15] R. Chau, B. Doyle, S. Datta, J. Kavalieros, and K. Zhang, “Integrated nanoelectronics for the future,” *Nature materials* **6**, 810–812 (2007).
- [16] B. Tian, X. Zheng, T. J. Kempa, Y. Fang, N. Yu, G. Yu, J. Huang, and C. M. Lieber, “Coaxial silicon nanowires as solar cells and nanoelectronic power sources,” *Nature* **449**, 885–889 (2007).
- [17] S. Cuenot, C. Frétiigny, S. Demoustier-Champagne, and B. Nysten, “Surface tension effect on the mechanical properties of nanomaterials measured by atomic force microscopy,” *Physical Review B* **69**, 165410 (2004).
- [18] S. Nilsson, E.-L. Sarwe, and L. Montelius, “Fabrication and mechanical characterization of ultrashort nanocantilevers,” *Applied physics letters* **83**, 990–992 (2003).
- [19] S. G. Nilsson, X. Borriese, and L. Montelius, “Size effect on young’s modulus of thin chromium cantilevers,” *Applied physics letters* **85**, 3555 (2004).
- [20] X. Li, T. Ono, Y. Wang, and M. Esashi, “Ultrathin single-crystalline-silicon cantilever resonators: fabrication technology and significant specimen size effect on young’s modulus,” *Applied Physics Letters* **83**, 3081–3083 (2003).
- [21] D. E. Armstrong, A. J. Wilkinson, and S. G. Roberts, “Measuring anisotropy in young’s modulus of copper using microcantilever testing,” *Journal of Materials Research* **24**, 3268–3276 (2009).

- [22] A. Krivtsov and N. Morozov, “Anomalies in mechanical characteristics of nanometer-size objects,” in *Doklady Physics*, Vol. 46 (Springer, 2001) pp. 825–827.
- [23] A. Krivtsov and N. Morozov, “On mechanical characteristics of nanocrystals,” *Physics of the solid state* **44**, 2260–2265 (2002).
- [24] E. Ivanova, A. Krivtsov, and N. Morozov, “Peculiarities of the bending-stiffness calculation for nanocrystals,” in *Doklady Physics*, Vol. 47 (Springer, 2002) pp. 620–622.
- [25] E. Ivanova, A. Krivtsov, and N. Morozov, “Bending stiffness calculation for nanosize structures,” *Fatigue & Fracture of Engineering Materials & Structures* **26**, 715–718 (2003).
- [26] D. C. Rapaport, *The art of molecular dynamics simulation* (Cambridge university press, 2004).
- [27] E. B. Tadmor and R. E. Miller, *Modeling materials: continuum, atomistic and multiscale techniques* (Cambridge University Press, 2011).
- [28] P. Heino, H. Häkkinen, and K. Kaski, “Molecular-dynamics study of mechanical properties of copper,” *EPL (Europhysics Letters)* **41**, 273 (1998).
- [29] L. Zhou and H. Huang, “Are surfaces elastically softer or stiffer?” *Applied Physics Letters* **84**, 1940–1942 (2004).
- [30] Y.-H. Wen, Z.-Z. Zhu, G.-F. Shao, and R.-Z. Zhu, “The uniaxial tensile deformation of ni nanowire: atomic-scale computer simulations,” *Physica E: Low-dimensional Systems and Nanostructures* **27**, 113–120 (2005).
- [31] H. S. Park and J. A. Zimmerman, “Modeling inelasticity and failure in gold nanowires,” *Physical Review B* **72**, 054106 (2005).
- [32] J. Diao, K. Gall, and M. L. Dunn, “Atomistic simulation of the structure and elastic properties of gold nanowires,” *Journal of the Mechanics and Physics of Solids* **52**, 1935–1962 (2004).
- [33] F. Streit, K. Sieradzki, and R. Cammarata, “Elastic properties of thin fcc films,” *Physical Review B* **41**, 12285 (1990).
- [34] H. Liang, M. Upmanyu, and H. Huang, “Size-dependent elasticity of nanowires: nonlinear effects,” *Physical Review B* **71**, 241403 (2005).

- [35] P. Villain, P. Beauchamp, K. Badawi, P. Goudeau, and P.-O. Renault, “Atomistic calculation of size effects on elastic coefficients in nanometre-sized tungsten layers and wires,” *Scripta materialia* **50**, 1247–1251 (2004).
- [36] H. Wu, “Molecular dynamics study on mechanics of metal nanowire,” *Mechanics Research Communications* **33**, 9–16 (2006).
- [37] H. Wu, “Molecular dynamics study of the mechanics of metal nanowires at finite temperature,” *European Journal of Mechanics-A/Solids* **25**, 370–377 (2006).
- [38] H. Wu, “Molecular dynamics simulation of loading rate and surface effects on the elastic bending behavior of metal nanorod,” *Computational materials science* **31**, 287–291 (2004).
- [39] J. Q. Broughton, C. A. Meli, P. Vashishta, and R. K. Kalia, “Direct atomistic simulation of quartz crystal oscillators: Bulk properties and nanoscale devices,” *Physical Review B* **56**, 611 (1997).
- [40] A. Ahadi and S. Melin, “Size dependence of the poisson’s ratio in single-crystal fcc copper nanobeams,” *Computational Materials Science* **111**, 322–327 (2016).
- [41] D. Johansson, P. Hansson, and S. Melin, “Stress analysis around a through crack shaped void in a single crystal copper strip coated on an infinitely stiff material using molecular dynamics,” *Engineering Fracture Mechanics* **116**, 58–68 (2014).
- [42] D. Johansson, P. Hansson, and S. Melin, “Stress analysis of highly constrained copper strips with through crack shaped voids using molecular dynamics,” in *Key Engineering Materials*, Vol. 592 (Trans Tech Publ, 2014) pp. 43–46.
- [43] D. Johansson, P. Hansson, and S. Melin, “Stress and displacement configurations in the vicinity of a void in a nanometer copper strip,” *Engineering Fracture Mechanics* **152**, 139–146 (2015).
- [44] W. Kim and M. Cho, “Surface effect on the self-equilibrium state and size-dependent elasticity of fcc thin films,” *Modelling and Simulation in Materials Science and Engineering* **18**, 085006 (2010).
- [45] J. S. Cho, H.-K. Kang, S. S. Wong, and Y. Shacham-Diamand, “Electroless cu for vlsi,” *MRS Bulletin* **18**, 31–38 (1993).

- [46] L. Magagnin, R. Maboudian, and C. Carraro, “Selective deposition of thin copper films onto silicon with improved adhesion,” *Electrochemical and Solid-State Letters* **4**, C5–C7 (2001).
- [47] S. Murugesan, J. T. Harris, B. A. Korgel, and K. J. Stevenson, “Copper-coated amorphous silicon particles as an anode material for lithium-ion batteries,” *Chemistry of Materials* **24**, 1306–1315 (2012).
- [48] H. Chen, Y. Xiao, L. Wang, and Y. Yang, “Silicon nanowires coated with copper layer as anode materials for lithium-ion batteries,” *Journal of power sources* **196**, 6657–6662 (2011).
- [49] V. A. Sethuraman, K. Kowolik, and V. Srinivasan, “Increased cycling efficiency and rate capability of copper-coated silicon anodes in lithium-ion batteries,” *Journal of Power Sources* **196**, 393–398 (2011).
- [50] M. Au, Y. He, Y. Zhao, H. Ghassemi, R. S. Yassar, B. Garcia-Diaz, and T. Adams, “Silicon and silicon–copper composite nanorods for anodes of li-ion rechargeable batteries,” *Journal of Power Sources* **196**, 9640–9647 (2011).
- [51] W. Wu, F. Huang, Y. Li, S. Zhang, X. Han, Z. Li, Y. Hao, and Y. Wang, “Rf inductors with suspended and copper coated thick crystalline silicon spirals for monolithic mems lc circuits,” *IEEE microwave and wireless components letters* **15**, 853–855 (2005).
- [52] D. Frenkel and B. Smit, *Understanding molecular simulations: From Algorithms to applications*, 2nd ed., ISBN-10: 0122673514 ISBN-13: 978-0122673511 (Academic Press, 2002).
- [53] M. P. Allen, “Introduction to molecular dynamics simulation,” *Computational soft matter: from synthetic polymers to proteins* **23**, 1–28 (2004).
- [54] M. P. Allen and D. J. Tildesley, *Computer simulation of liquids* (Oxford university press, 1989).
- [55] J.-P. Hansen and I. R. McDonald, *Theory of simple liquids*, 3rd ed. (Academic Press, 2006) iISBN-13: 9780123705358 ISBN-10: 0123705355.
- [56] H. Goldstein, C. P. J. Poole, and J. L. Safko, *Classical Mechanics*, 3rd ed. (Pearson, 2001) iISBN-13: 978-0201657029 ISBN-10: 0201657023.
- [57] W. Qiu-Dong, “The global solution of the n-body problem,” *Celestial Mechanics and Dynamical Astronomy* **50**, 73–88 (1990).

- [58] F. Diacu, “The solution of the n-body problem,” *The Mathematical Intelligencer* **18**, 66–70 (1996).
- [59] D. V. Schroeder, *An introduction to thermal physics*, Vol. 60 (Addison Wesley New York, 2000).
- [60] J. E. Jones, “On the determination of molecular fields. ii. from the equation of state of a gas,” in *Proceedings of the Royal Society of London A: Mathematical, Physical and Engineering Sciences*, Vol. 106 (The Royal Society, 1924) pp. 463–477.
- [61] J. Li, X. Dai, S. Liang, K. Tai, Y. Kong, and B. Liu, “Interatomic potentials of the binary transition metal systems and some applications in materials physics,” *Physics Reports* **455**, 1–134 (2008).
- [62] A. E. Carlsson, “Beyond pair potentials in elemental transition metals and semiconductors,” *Solid State Physics* **43**, 1–91 (1990).
- [63] M. S. Daw, S. M. Foiles, and M. I. Baskes, “The embedded-atom method: a review of theory and applications,” *Materials Science Reports* **9**, 251–310 (1993).
- [64] M. I. Baskes, “Modified embedded-atom potentials for cubic materials and impurities,” *Physical Review B* **46**, 2727 (1992).
- [65] M. Baskes, “Modified embedded atom method calculations of interfaces,” Report number: SAND-96-8484C, Sandia National Laboratories, Livermore (1996).
- [66] M. S. Daw and M. I. Baskes, “Semiempirical, quantum mechanical calculation of hydrogen embrittlement in metals,” *Physical review letters* **50**, 1285 (1983).
- [67] M. S. Daw and M. I. Baskes, “Embedded-atom method: Derivation and application to impurities, surfaces, and other defects in metals,” *Physical Review B* **29**, 6443 (1984).
- [68] M. Baskes, J. Nelson, and A. Wright, “Semiempirical modified embedded-atom potentials for silicon and germanium,” *Physical Review B* **40**, 6085 (1989).
- [69] B. Jelinek, S. Groh, M. F. Horstemeyer, J. Houze, S.-G. Kim, G. J. Wagner, A. Moitra, and M. I. Baskes, “Modified embedded atom method potential for al, si, mg, cu, and fe alloys,” *Physical Review B* **85**, 245102 (2012).

- [70] Z. Tang, M. Hasegawa, Y. Nagai, and M. Saito, “Density functional study on metastable bcc copper: Electronic structure and momentum density of positron-electron pairs,” *Physical Review B* **65**, 195108 (2002).
- [71] T. Leung, W. Lee, and X. Lu, “Diamond turning of silicon substrates in ductile-regime,” *Journal of materials processing technology* **73**, 42–48 (1998).
- [72] F. Ebrahimi and L. Kalwani, “Fracture anisotropy in silicon single crystal,” *Materials Science and Engineering: A* **268**, 116–126 (1999).
- [73] E. J. Boyd and D. Uttamchandani, “Measurement of the anisotropy of young’s modulus in single-crystal silicon,” *Journal of Microelectromechanical Systems* **21**, 243–249 (2012).
- [74] V. Kaajakari, “Silicon as an anisotropic mechanical material-a tutorial,” (2002).
- [75] G. Dienes and A. Paskin, “Molecular dynamic simulations of crack propagation,” *Journal of Physics and Chemistry of Solids* **48**, 1015–1033 (1987).
- [76] A. Mayer and V. Krasnikov, “Copper spall fracture under sub-nanosecond electron irradiation,” *Engineering Fracture Mechanics* **78**, 1306–1316 (2011).
- [77] Sandia, “Lammps (svn 13475),” (2015), <http://lammps.sandia.gov/>.
- [78] A. Garg, A. Acharya, and C. E. Maloney, “A study of conditions for dislocation nucleation in coarser-than-atomistic scale models,” *Journal of the Mechanics and Physics of Solids* **75**, 76–92 (2015).
- [79] G. Ziegenhain, A. Hartmaier, and H. M. Urbassek, “Pair vs many-body potentials: Influence on elastic and plastic behavior in nanoindentation of fcc metals,” *Journal of the Mechanics and Physics of Solids* **57**, 1514–1526 (2009).
- [80] T. L. Anderson, *Fracture mechanics: fundamentals and applications*, 2nd ed. (CRC press, 2000 N. W. Corporate Blvd., Boca Raton, Florida 33431, 1995).

